

PAPER • OPEN ACCESS

Dislocation sub-structures, recovery and recrystallization in pure tantalum

To cite this article: C Moussa *et al* 2022 *IOP Conf. Ser.: Mater. Sci. Eng.* **1249** 012062

View the [article online](#) for updates and enhancements.

You may also like

- [3D microstructural evolution of primary recrystallization and grain growth in cold rolled single-phase aluminum alloys](#)
Khaled Adam, Dana Zöllner and David P Field
- [A comprehensive method to identify the kinetics of static recrystallization using the hot torsion test results with an inverse solution](#)
S Khoddam and P D Hodgson
- [Kinetics of recrystallization and microstructure distribution during isothermal annealing of cold rolled nickel](#)
N Jahani, M Reihanian and Kh Gheisari



ECS
The
Electrochemical
Society
Advancing solid state &
electrochemical science & technology

DISCOVER
how sustainability
intersects with
electrochemistry & solid
state science research

Dislocation sub-structures, recovery and recrystallization in pure tantalum

C Moussa¹, J Baton¹ and W Geslin²

¹ MINES ParisTech, PSL Research University, CEMEF - Centre de mise en forme des matériaux, CNRS UMR 7635, CS 10207 rue Claude Daunesse, 06904 Sophia Antipolis Cedex, France

² CEA DAM Valduc, F-21120 Is-sur-Tille, France

E-mail: charbel.moussa@mines-paristech.fr

Abstract. Plastic deformation, static recovery and recrystallization in pure tantalum are analyzed in the present paper. Quantitative analysis of dislocation sub-structures were done. Sub-structures development is completely dependent on crystallographic orientation. No clear effect of recovery was observed when direct analysis was made. Hence, recovery was studied through its effect on recrystallization. Recovery heat treatments followed by a recrystallization heat treatment were applied to compare the recrystallized state of samples which were subject to prior recovery with those which were not. Results show that recrystallization is accelerated in the early stages of recovery (low temperature or low annealing time or low plastic strain). On the opposite, in the advanced stages of recovery, it slows down recrystallization. Results show again an influence of crystallographic orientation. Static recrystallization was also investigated and the influence of crystallographic orientation, most probably inherited from the deformed state through dislocation sub-structures, was observed. Based on experimental results, a discussion on the mechanisms of nucleation in the different orientation grains is presented. Finally, a discussion is made on the quantification of stored energy. The effect of the observation scale and the choices of considering dislocation density or dislocation sub-boundaries energies from EBSD data is discussed.

1. Introduction

Tantalum is a Body Centered Cubic (bcc) metal with three slip systems: $\{110\}\langle 111\rangle$, $\{112\}\langle 111\rangle$ and $\{123\}\langle 111\rangle$. Even though tantalum slips mainly on $\{110\}$ planes during cold deformation, it may also slip on planes with maximal resolved shear stress [1]. In bcc materials, cross slip can easily take place since no stable stacking faults were observed [2]. Many experimental evidence on dislocation sub-structures in bcc materials can be found [3,4]. Influence of crystallographic orientation on dislocation densities and sub-structures in bcc materials was observed [5]. More sub-structures and higher stored energy were observed in grains with $\langle 111\rangle$ direction parallel to normal direction (ND) than in grains with $\langle 100\rangle$ direction parallel to ND on cold rolled tantalum [6].

The influence of crystallographic orientation on the stored energy directly influences subsequent recrystallization. It was reported that nucleation is favored in grains with dislocation sub-structures in tantalum [7]. For estimating stored energy from Electron Back Scatter Diffraction (EBSD), several methods can be used [8]. Generally, the stored energy is calculated either as the sum of the energies of all individual dislocations or as the sum of the energies of the sub-boundaries.



Because of the ease of cross slip in bcc materials, recovery can take place. It is generally accepted that recovery, which is activated at lower temperatures, tends to slow down recrystallization kinetics. However, some studies showed that recovery may enhance recrystallization such in aluminum alloys [9]. Less studies were made on recovery in bcc materials.

The current paper is a synthesis of new findings on microstructure evolutions in pure tantalum during plastic deformation [10], recrystallization [11] and recovery [12]. Special focus is made on the effect of crystallographic orientation on sub-structures development and their effect on recrystallization and recovery through EBSD analysis at the polycrystalline and at the sub-structures' scales.

2. Material presentation and experimental conditions

High purity (>99.99% wt.) tantalum sheet was used in the present study. EBSD maps used for the analysis at the polycrystalline scale and at the substructures scale were made with a step size of 1.2 μm and 90 nm respectively. Quantitative EBSD analysis was performed using homemade routines within the MTEX toolbox [13]. The microstructure of the as received material in the center of the sheet and in the quarter layer region are presented in figure 1(a). The fully recrystallized microstructure is very different in the two regions. In the center of the sheet, upper part of figure 1(a), a dominant γ -fiber (<111> direction parallel to ND) of around 70-80% of volume fraction can be observed. In the quarter layer region, lower part of figure 1(a), γ -fiber represents about 10% and θ -fiber (<100> direction parallel to ND) about 30%. Those textures are inherited from the last rolling steps with a strong shear component near the surface because of friction and mainly compressive components in the center of the sheet. A more detailed texture analysis with X-ray diffraction can be found in [10]. In this study, all grains (grain boundaries defined with a disorientation higher than 10°) were classified into three groups: γ -fiber, θ -fiber and "others" for the grains that do not belong to either of the first two classes. The material corresponding to the center, upper part of figure 1, and the one corresponding to the quarter layer, lower part of figure 1, are called AR1 and AR2 (for as-received).

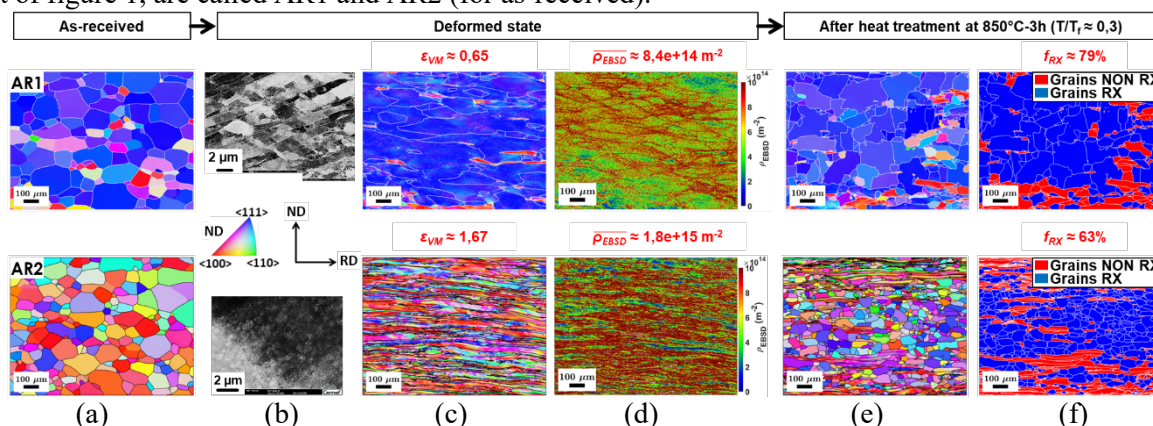


Figure 1. Upper part for AR1 and lower part for AR2. (a) EBSD maps of the as-received materials [10], (b) Electron Channeling Contrast Imaging (ECCI) micrographs of the deformed state [10], (c) EBSD maps after plastic deformation [10], (d) dislocation density ρ_{EBSD} maps [12], (e) EBSD maps after heat treatment [11] and (f) Grain Orientation Spread maps differentiating recrystallized and non-recrystallized grains (RD stands for Rolling direction).

3. Dislocation sub-structures in cold deformed tantalum

3.1. Polycrystalline scale analysis

To study sub-structures development during plastic deformation, AR1 was deformed by compression (parallel to ND) and AR2 by cold rolling [10]. For more details on deformation conditions and texture evolutions please report to [10]. Dislocation density ρ_{EBSD} was estimated from EBSD data using the Nye's tensor with the method proposed by Pantleon [14]. The deformed microstructures along with ρ_{EBSD} maps for $\varepsilon_{VM} = 0.65$ for the AR1 and $\varepsilon_{VM} = 1.67$ for the AR2 are presented in figures 1(c) and

1(d). As illustrated in figure 2(a), the evolution of the average dislocation density ($\overline{\rho_{EBSD}}$) in function of ε_{VM} is different for each class of orientations. $\overline{\rho_{EBSD}}$ is higher in the γ -fiber grains than in the θ -fiber grains of around 60% with a faster increase. $\overline{\rho_{EBSD}}$ in “other” grains is either between those of γ -fiber and θ -fiber grains or close to those of γ -fiber for others. This observation is consistent with the average Taylor factor of each class, 3.5, 2.4 and 3.0 for γ -fiber, θ -fiber and “other” grains respectively. However, no correlation was found between $\overline{\rho_{EBSD}}$ and the Taylor factor grain per grain. $\overline{\rho_{EBSD}}$ is higher in the γ -fiber grains of the AR1 than in those of the AR2 as illustrated in figure 2(b). This is probably due to interactions with neighboring grains as it will be discussed in the next section.

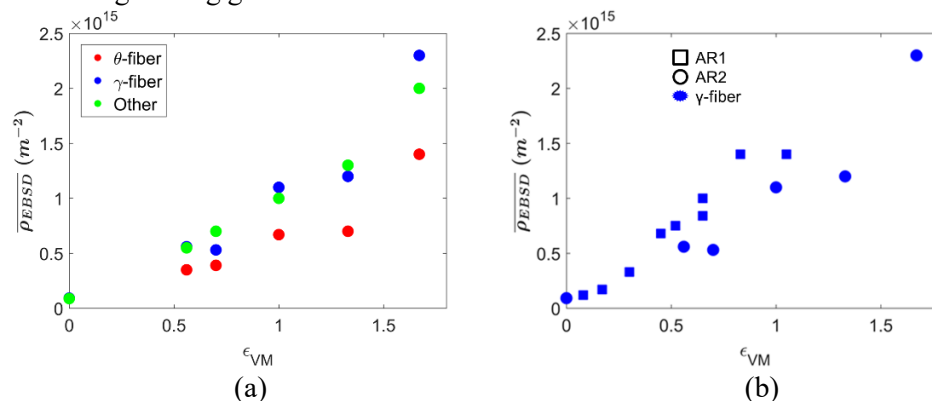


Figure 2. Evolution of $\overline{\rho_{EBSD}}$ with ε_{VM} (a) for each class of orientations and (b) for the γ -fiber grains in AR1 and AR2 [10].

3.2. Dislocation substructures' scale analysis

To analyze dislocation substructures evolution in the grains of each class, Electron Channeling Contrast Imaging (ECCI) micrographs were made in the γ -fiber and θ -fiber grains as illustrated in figure 1(b). The micrograph in the upper part of figure 1(b) was obtained in a γ -fiber grain in AR1 and the one in the lower part of figure 1(b) was obtained in a θ -fiber grain in AR2. Figure 1(b) shows that sub-structures are formed in the γ -fiber grains even for small ε_{VM} (even at $\varepsilon_{VM} = 0.3$ [10]). As for θ -fiber grains, very few sub-structures were observed even for $\varepsilon_{VM} = 1.67$. This observation agrees with the observations made at the polycrystalline scale where $\overline{\rho_{EBSD}}$ is higher in the γ -fiber grains (figure 2(a)).

For the analysis of dislocation sub-structures EBSD maps were acquired with a step size of 90 nm. All segments with a disorientation between 1.5° and 10° were considered as sub-boundaries. They are quantified through their average disorientation $\overline{\theta_{sub}}$ and their density $\overline{\rho_{sub}}$ (total length of sub-boundaries over total area ratio). For statistical details please refer to [10].

The evolutions of $\overline{\theta_{sub}}$ and $\overline{\rho_{sub}}$ in function of ε_{VM} for the three orientation classes are presented in figures 3(a) and 3(b) respectively. As expected, $\overline{\theta_{sub}}$ and $\overline{\rho_{sub}}$ are higher in the γ -fiber grains than in the “other” oriented grains which in their turn are higher than in the θ -fiber grains. To describe the evolution of $\overline{\theta_{sub}}$ and $\overline{\rho_{sub}}$ in function of ε_{VM} , power laws were used for every case as illustrated in figure 3. The obtained laws are not in agreement with the ones proposed in [15] on aluminum for Geometrically Necessary Boundaries (GNB) and Incidental Dislocation Boundaries (IDB). One possible explanation of such differences is that the proposed laws on face centered cubic aluminum may not be suitable to describe sub-structures evolution in bcc tantalum.

From figure 3(b), it can be observed that for AR1, with a dominant γ -fiber ≈ 70 -80%, the development of sub-boundaries occurs for small ε_{VM} and an early saturation appears (additional experiments for higher ε_{VM} would confirm this saturation at $\overline{\rho_{sub}} \approx 2 \mu m^{-1}$). For AR2, with less γ -fiber $\approx 10\%$, figure 3(b) shows that $\overline{\rho_{sub}}$ keeps increasing even with high ε_{VM} with no saturation indicating a continuous sub-structures development with ε_{VM} . In addition, sub-structures development seems more homogenous (smaller error bars) in the case of AR1 than in the case of AR2. Those two observations illustrate the influence of the neighboring grains (majority of γ -fiber for AR1) on substructures development in γ -

fiber grains. Hence, even though the grain orientation is of prime importance, the neighboring grain orientations also affect the plastic deformation of grains.

No correlation between orientation long range gradients and crystallographic orientation was found [10].

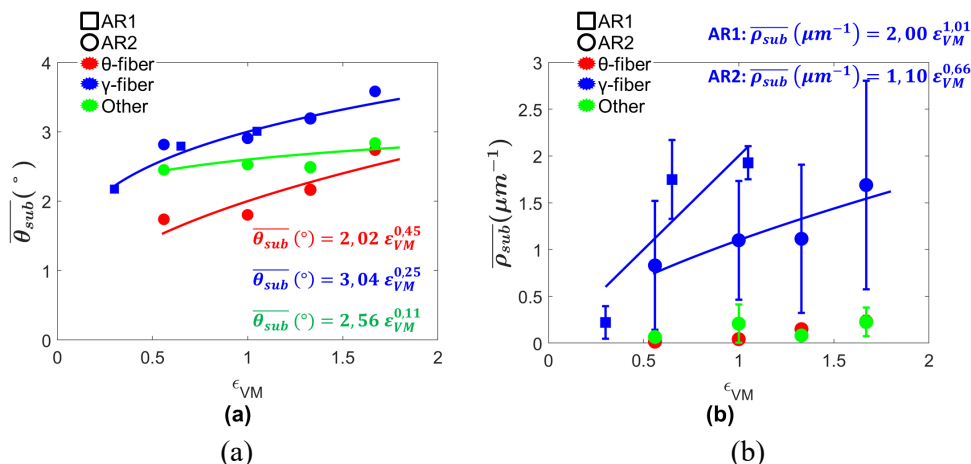


Figure 3. Evolution of (a) $\overline{\theta_{sub}}$ and (b) $\overline{\rho_{sub}}$ in function of ϵ_{VM} for the three orientation classes. Power laws were used to fit experimental data [10].

4. Static recrystallization in pure tantalum

As illustrated in figures 1(e) and 1(f) recrystallization is much faster in AR1 than in AR2 even with smaller ϵ_{VM} . This faster recrystallization is due to the high amount of stored energy despite smaller ϵ_{VM} . As illustrated in figure 2(a) dislocation density is higher in the γ -fiber grains which explains the high $\overline{\rho_{EBSD}}$ in AR1 than in AR2 for a given ϵ_{VM} . The evolution of the recrystallized fraction for the three classes of orientation is presented in figure 4(a) and 4(b) for AR1 and AR2 respectively. Recrystallized grains mainly belong to the γ -fiber class. This crystallographic orientation of recrystallized grains is inherited from the deformed state. Because of well-formed sub-structures, figures 1(b) and 3, nucleation is enhanced in γ -fiber grains and diminished in θ -fiber grains. Hence, deformed θ -fiber grains are mainly consumed by recrystallized grains issued from neighboring γ -fiber grains than by those who nucleate in the deformed θ -fiber grains. This hypothesis is supported by the faster evolution of γ -fiber recrystallized grains volume fraction observed in figures 4(a) and 4(b). It can be also concluded that grains which recrystallize in the deformed γ -fiber grains are probably γ -fiber oriented.

The grain sizes values, presented in figures 4(a) and 4(b), show higher grain sizes for γ -fiber recrystallized grains for AR1 and AR2. A faster nucleation (shorter incubation time) as a result of the sub-structures in the deformed state explains this observation.

The comparison between figures 4(a) and (b) shows that recrystallized grain sizes in AR1 are bigger than in AR2. Two possible reasons may explain this difference. The first one is the faster nucleation in the γ -fiber deformed grains (dominant in AR1) leading to additional growth time and size advantage from the early stages of the annealing. The second one is the deformed grains morphology (figure 1(c)) where the deformed AR1 has almost three times less grain boundaries than the deformed AR2 ($0,06\mu\text{m}/\mu\text{m}^2$ and $0,175\mu\text{m}/\mu\text{m}^2$ respectively). Considering that grain boundaries are potential nucleation sites, more nuclei may appear in the deformed AR2 leading to a smaller recrystallized grain size.

It is important to mention, that when $\overline{\rho_{EBSD}}$ estimated at the polycrystalline scale (step size of $1,2\mu\text{m}$) was used to quantify stored energy, contradictory results were obtained. For example, the values of $\overline{\rho_{EBSD}}$ given in figure 1(d) are contradictory with those of recrystallized fraction in figure 1(f). However, when EBSD data at the sub-structures scale (step size of 90 nm) were used, $\overline{\rho_{EBSD}}$ gave consistent results. This observation is probably because Geometrically Necessary Dislocation (GND) density is correctly estimated with EBSD data acquired at the sub-structures scale [16]. Independently of the scale

analysis, results showed that the quantification of the stored energy using the dislocation sub-structures [8] instead of $\overline{\rho}_{EBSD}$ gave more consistent results with recrystallized fractions [11].

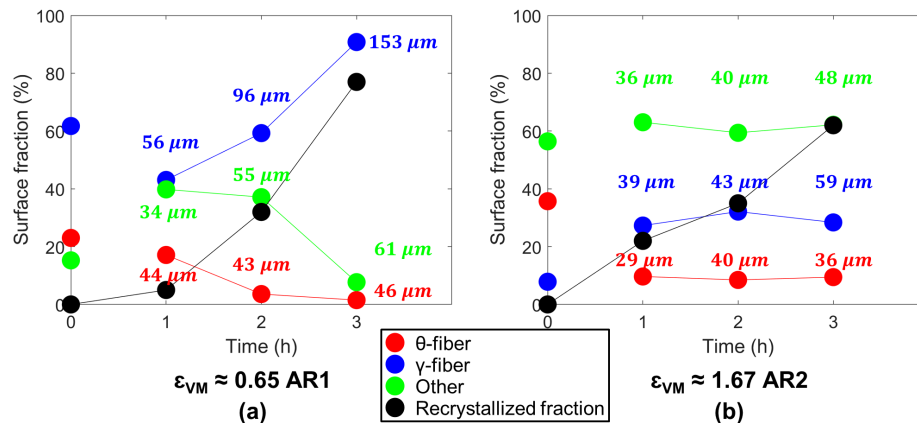


Figure 4. Evolution of the surface fraction of each class of orientations among recrystallized fraction (black curve) with annealing time for (a) AR1 and (b) AR2. The given values correspond the average recrystallized grain size [11].

5. Recovery in pure tantalum

Because of the ease of cross slip in tantalum, recovery is expected to take place and to influence recrystallization. Therefore, AR2 samples deformed up to $\epsilon_{VM} = 0.56, 1.00$ and 1.67 were submitted to a recovery heat treatment at 750°C for 4 hours. Then samples were analyzed through hardness measurements, $\overline{\rho}_{EBSD}$, $\overline{\theta}_{sub}$ and $\overline{\rho}_{sub}$ [12]. No clear evolution induced by recovery was observed.

Therefore, it was decided to analyze recovery indirectly through its effect on recrystallization. A one stage recrystallization heat treatment (950°C for 30 min.) and five two stages heat treatment of pre-recovery (700°C for 60 min., 750°C for 15 min., 750°C for 60 min., 750°C for 240 min. and 800°C for 60 min.) followed by a recrystallization heat treatment (950°C for 30 min.) were done without any cooling between the two treatments. The recrystallized fractions are reported in figures 5(a) and 5(b) in function of the temperature and the time of the pre-recovery treatment respectively. For all the cases, pre-recovery affects recrystallized fraction indicating that recovery is indeed activated.

Recovery is known to decrease the stored energy because of annihilation of redundant dislocations and therefore to slow-down recrystallization. In the present case, this was observed for the major cases with a smaller recrystallized fraction for samples subject to pre-recovery when compared to the samples which were not subject to pre-recovery, figure 5. However, for the three cases circled in figures 5(a) and 5(b), recovery enhanced recrystallization with a higher recrystallized fraction.

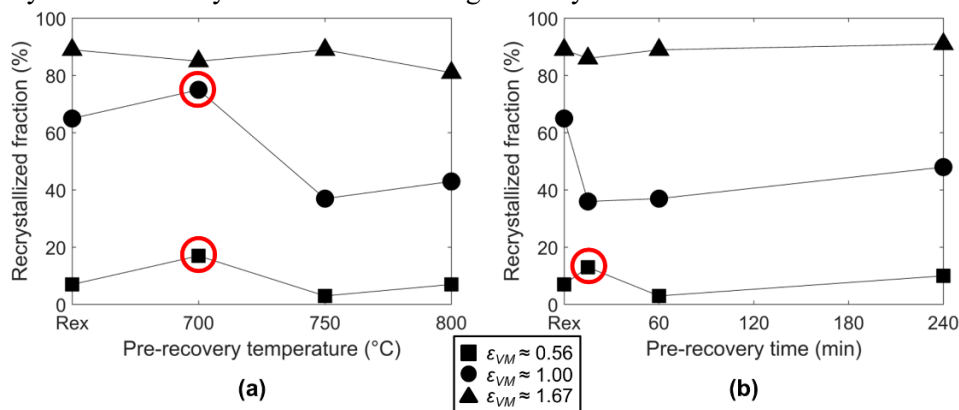


Figure 5. Recrystallized fraction in function of pre-recovery (a) temperature (for 60 min.) and (b) time (at 750°C) treatment followed by a recrystallization treatment at 950°C for 30 min. estimated from EBSD maps of $1.2 \text{ mm} \times 0.9 \text{ mm}$ [12].

These observations illustrate two competitive mechanisms occurring during recovery. The first one, associated with annihilation of dislocations and a decrease of stored energy; slows down recrystallization. The second mechanism consists in the increase of the ability of sub-structures to migrate by decreasing dislocations tangles around them. This mechanism would make nucleation faster by decreasing incubation time. Therefore, the effect of recovery depends on the balance between those two mechanisms. Results show that at the early stages of recovery (low temperature or short time or low plastic strain) the second mechanism is favored and recrystallization is accelerated. On the opposite, when recovery advances the first mechanism is dominant, and recrystallization is slowed down.

Additional analysis of the effect of recovery on the recrystallized grains size and their crystallographic orientation can be found in [12].

6. Conclusions

Plastic deformation, static recovery and recrystallization in pure tantalum were analyzed in the present paper. Several main conclusions can be reported.

- Dislocations sub-structures develop in γ -fiber grains even at low plastic strains unlike in θ -fiber grains where very few sub-structures were observed even at high plastic strain.
- When γ -fiber is dominant, dislocation sub-boundaries develop homogeneously from the early stages of deformation with a quick saturation and their disorientation continue to increase. When γ -fiber is not dominant, the appearance of new sub-boundaries with strain continues.
- The orientation dependence of plastic deformation influences recrystallization. Nucleation is enhanced in γ -fiber deformed grains giving place to mostly γ -fiber recrystallized grains. Hence, microstructure composed mainly of γ -fiber grains recrystallizes much faster.
- Estimation of stored energy using dislocation density estimated from EBSD at the polycrystalline scale gives contradictory results. For a more precise estimation, it is necessary to estimate stored energy from dislocation sub-boundaries from data acquired at sub-structures scale.
- Recovery gives place to two competitive mechanisms, one accelerating and one slowing down recrystallization. The first one is dominant at the early stages of recovery, the second one is dominant when recovery advances.

References

- [1] Weinberger C R, Boyce B L and Battaile C C 2013 *Int. Mater. Rev.* **58** 296–314
- [2] Hull D and Bacon D 2001 *Introduction to dislocations* (Oxford: Butterworth-Heinemann)
- [3] Moussa C, Bernacki M, Besnard R and Bozzolo N 2017 *Ultramicroscopy* **179** 63–72
- [4] Moussa C, Bernacki M, Besnard R and Bozzolo N 2015 *IOP Conf. Ser. Mater. Sci. Eng.* **89** 012038
- [5] Wauthier-Monnin A, Chauveau T, Castelnau O, Réglé H and Bacroix B 2015 *Mater. Charact.* **104** 31–41
- [6] Liu Y, Liu S, Deng C, Fan H, Yuan X and Liu Q 2018 *J. Mater. Sci. Technol.* **34** 2178–82
- [7] Sandim H R Z, Padilha A F, Randle V and Blum W 1999 *Int. J. Refract. Hard Met.* **17** 431–5
- [8] Godfrey A, Mishin O V and Yu T 2015 *IOP Conf. Ser. Mater. Sci. Eng.* **89** 012003
- [9] Ren X, Huang Y, Zhou W, Zhao L, Wang Q and Min X 2019 *Mater. Sci. Eng. A* **764** 138159
- [10] Baton J, Geslin W and Moussa C 2021 *Mater. Charact.* **171** 110789
- [11] Baton J, Geslin W and Moussa C 2022 *Int. J. Refract. Hard Met.* **104** 105786
- [12] Baton J, Geslin W and Moussa C 2021 *J. Mater. Sci.* **56** 15354–78
- [13] Bachmann F, Hielscher R and Schaeben H 2010 *Solid State Phenom.* **160** 63–8
- [14] Pantleon W 2008 *Scr. Mater.* **58** 994–7
- [15] Pantleon W 2001 *Mater. Sci. Eng. A* **319–321** 211–5
- [16] Ruggles T J, Rampton T M, Khosravani A and Fullwood D T 2016 *Ultramicroscopy* **164** 1–10